RSC Advances

PAPER

View Article Online
View Journal | View Issue



Cite this: *RSC Adv.*, 2024, **14**, 1822

# Physical properties of vacancy-ordered double perovskites $K_2TcZ_6$ (Z = Cl, Br) for spintronics applications: DFT calculations

Huda A. Alburaih,[a] Sadia Nazir,*[b] N. A. Noor,*[c] A. Laref[d] and M. Musa Saad H.-E.[e]

Vacancy-ordered double perovskites (DPs) are emerging materials for spintronics due to their stable structures and non-toxic properties. In this study, we conducted a comprehensive investigation into the role of 4d electrons in Tc to understand their impact on the ferromagnetic properties of $K_2TcY_6$ (Y = Cl, Br). We have employed a modified Back and Johnson potential to assess electronic and magnetic characteristics and utilized the BoltzTraP code to investigate thermoelectric effects. Experimental lattice constants confirmed the presence of stable structures and formation energy estimates affirmed their thermodynamic stability. The Heisenberg model and density of electron states (DOS) at the Fermi level provides insights into Curie temperature and spin polarization. The presence of ferromagnetism is evident in the density of states, reflecting the transition of electron spins that support the exchange mechanism. The study delves into how electron functionality influences the control of ferromagnetism, considering exchange constants, exchange energies, hybridization process and the crystal field energies. Moreover, the exploitation of magnetic moments from Tc to K and Cl/Br sites takes precedence in driving ferromagnetism by exchanging electron spins rather than forming magnetic clusters. Additionally, to explore the optical characteristics of the compounds, we investigated their optical absorption, dielectric constants and refractive index within the energy range of 0–10 eV, ensuring absorption across both the visible and ultraviolet regions. Finally, we delve into the impact of the thermoelectric effect on both thermoelectric performance and spin functionality, taking into account factors such as the Seebeck coefficient, power factor, and electronic conductivity.

Received 7th November 2023
Accepted 27th December 2023

DOI: 10.1039/d3ra07603b

rsc.li/rsc-advances



## 1. Introduction

Over the last two decades, there has been significant research interest in the field of room temperature ferromagnetism in semiconductors, primarily because of its potential applications in non-volatile memory, quantum computing and spintronics.[1–5] Ferromagnetism in semiconductors holds the promise of facilitating the transmission of spin-polarized electrons, a crucial requirement in spintronics.[6] Initial reports suggesting the possibility of a Curie temperature above room temperature in materials like GaN and ZnO[7] led to several experimental studies claiming the existence of room temperature ferromagnetism.[8–11] Furthermore, ferromagnetism has been identified in a range of non-magnetic semiconductor samples through the introduction of the creation of atomic defects and non-magnetic elements.[12–21] This phenomenon is commonly referred to as $d^0$ ferromagnetism.[22] In such cases, the source of magnetism is distinct from the partially filled 4d or f-orbital electrons. The investigation of ferromagnetic characteristics has become a technological necessity for future advancements, given that spin-polarized currents have the ability to flow, unlike the unpolarized currents found in traditional electronic devices. As a result, researchers have reported the presence of ferromagnetic characteristics in perovskite materials.[23] However, the applicability of perovskites on a broader scale is hindered by the presence of toxic constituent elements and stability concerns.[24]

To address these limitations, researchers have undertaken studies on ferromagnetism in various $A_2BB'X_6$ type double perovskites (DPs).[25–27] The half-metallic DP $Sr_2FeMoO_6$ has demonstrated a magnetic transition at temperature 410 K, as reported in ref. 28. This finding highlights the potential of such materials to unveil magnetic characteristics at higher temperatures.[28] In a more recent experimental study of $Pr_2FeCrO_6$, researchers observed a magnetic transition occurring at 550 K. This finding was supported by the observed changes in

[a]*Physics Department, College of Science, Princess Nourah Bint Abdulrahman University, 11671 Riyadh, 12211, Saudi Arabia*
[b]*Department of Physics, University of Lahore, Pakistan*
[c]*Department of Physics, RIPHAH International University, Campus Lahore, Pakistan. E-mail: naveedcssp@gmail.com*
[d]*Department of Physics and Astronomy, College of Science, King Saud University, Riyadh, 11451, King Saudi Arabia*
[e]*Department of Physics, College of Science and Arts in Al-Muthnib, Qassim University, Al-Muthnib 51931, Saudi Arabia*

magnetic susceptibility, dielectric constant and resistivity as a function of temperature.[29,30] Double perovskite materials have been extensively explored for their magnetic and thermoelectric characteristics using a Density Functional Theory (DFT) approach, including compounds like $Ba_2FeMoO_6$ and $Dy_2CoMnO_6$.[31,32] Double perovskite structures with a vacancy ordering are created by replicating the conventional $ABX_3$ perovskite configuration and subsequently eliminating half of the B-type cations.[33] These DPs are appealing because of their resemblance to perovskites in terms of structure and their impressive material characteristics, stemming from their broad range of constituent ion compositions and the potential for tilting in the $[BX_6]^{2-}$ octahedra.[34–36] Recently, DPs with cubic vacancy ordering in the $A_2BX_6$ structure have been employed in light absorption applications.[37]

Researchers are also engaged in theoretical investigations of these vacancy-ordered DPs to explore their half-metallic ferromagnetic characteristics.[38] Moreover, vacancy-ordered DPs with ferromagnetic properties are worth exploring for potential applications in thermoelectric systems.[39] Using DFT calculations, spin dependent DPs $Rb_2(Tc,Mo)X_6$ (X = Cl, Br) are investigated for spintronic applications due to the role of Mo/Tc atom 4d electrons and show all DPs ferromagnetic characteristics.[40] Mustafa *et al.*,[41] systematically explored the ferromagnetic characteristics in DPs $Rb_2(Os/Ir)Cl/Br_6$ using density functional theory. Their analysis of the computations shows that electron spin causes ferromagnetism to be induced by crystal field energy. The structural formula of $K_2TcY_6$ (Y = Cl or Br) suggests the potential for ferromagnetism in these vacancy-ordered DPs. These investigated DPs are gaining prominence as novel materials in the realm of spintronic applications, including the realization of phenomena such as dynamic random-access memories (DRAM), swift quantum computing, spin valves, magnetic switches and the giant magnetoresistance effect (GMR). In such devices, properties are controlled by manipulating the spin of electrons rather than altering their charge, making these materials faster and more versatile. Additionally, these materials find use in power-harvesting tools such as thermoelectric generators.

The investigation of these DPs is motivated by their full spin polarization, substantial magnetic coupling and enduring ferromagnetism, making them promising candidates for spintronic devices. Particularly, these DPs present the intriguing feature of maintaining ferromagnetic properties at temperatures exceeding room temperature, while simultaneously exhibiting ultralow thermal conductivity.[42,43] Moreover, $Cs_2AgFeCl_6$ is subjected to magnetic and transport analysis employing the TB-mBJ potential, and its thermoelectric features are elucidated through a figure of merit scale.[44,45] This study includes the comprehensive first-principles calculations to explore the magnetic characteristics within the DPs $K_2TcY_6$ (Y = Cl, Br). Experimental findings[46] regarding $K_2TcY_6$ suggest that the Tc atom is a promising candidate for generating a substantial magnetic moment and ferromagnetic spin ordering in initially non-magnetic materials. Consequently, the $K_2TcY_6$ (Y = Cl, Br) DPs may exhibit intriguing electronic properties, which could play a crucial role in advancing the field of spintronics within these direct bandgap semiconductors. We have further examined the impact of their ferromagnetic nature on the thermoelectric properties by analyzing key thermoelectric parameters computed using the BoltzTraP code.[47] Moreover, our results clearly demonstrate semiconducting ferromagnetic nature of these compounds and ultralow values of $\kappa_e$ that can prove useful for application of these materials in spintronic and thermoelectric devices.

## 2. Method of calculations

The DFT gives the absolute information of the compounds' properties before recognizing them for being utilized in useful manufacturing of various devices. BoltzTraP codes were brought into use for thermoelectric analysis whereas the Wien2k code[48] was employed for the evaluation of the structural, magnetic and spin-polarized electronic features. The optimization for AFM and FM states along with structural properties were conducted by PBEsol in the FP-LAPW method.[49] Although the PBEsol accurately determines the lattice parameters as well as the energies of the system, it is unable to evaluate their band gaps and electronic behavior. For that reason, TB-mBJ potential were employed as an entire package for the improvement of band gap on which the compounds' physical features relies.[50] In the whole potential method, the electronic gap system was divided into interstitial regions and muffin-tin corresponding to the plane wave and spherical harmonic solutions. In addition, $R_{MT} \times K_{max} = 8.0$ was set by holding the radius of the muffin tin sphere as well as the wave vector in the opposite lattice. A $k$-mesh of $20 \times 20 \times 20$ was employed for the iterative energy conversion approach within the first Brillouin zone. The above-mentioned $k$-mesh performed the convergence of the whole observed system. As a default setup, the other two fundamental factors such as angular momentum $\ell_{max} = 10$ and Gaussian factor $G_{max} = 16$. The convergence of energy was the sequence of $10^{-4}$ Ry. The charge convergence obtained from TB-mBJ, alongside the ground state energy, serves as the input for the BoltzTraP code, a classical transport theory-based tool for studying transport properties.

## 3. Results and discussion

### 3.1 Structural properties

Fig. 1 shows the structural nature of the observed compounds ($Fm\bar{3}m$ (225)) in cubic phase. The left part in the Fig. 1 presents the polyhedral form whereas the right one displays ball format. The geometric and atomic configurations are ensured by the unit cell. Amongst the octahedral of $M(Cl/Br)_6$, the K atoms are located. The octahedral form for every atom is kept by the 12-fold composition order of Cl/Br atoms. The Tc atoms lie in the middle position of every octahedron of Cl/Br atoms. Further, the Wyckoff positions for Tc, Cl/Br and K are 4a (0, 0, 0), 24e (0.20, 0, 0), and 8c (0.25, 0.25, 0.25), respectively. The obtained values of the lattice constants ($a_0$) determined through Murnaghan equation of state and found comparable to experimental lattice constant.[46] From Table 1, it is clear when the ionic radius increases, the $a_0$ also starts increasing from Cl to Br containing

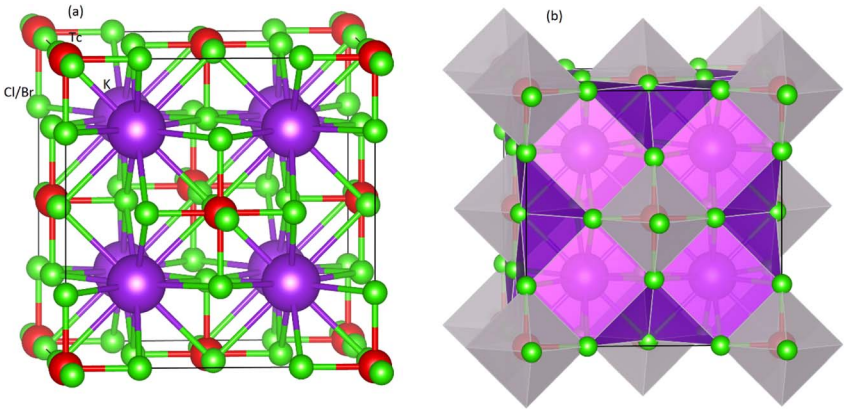


Fig. 1 Unit cell of double perovskites $K_2TcX_6$ (X = Cl, Br) (a) ball format and (b) polyhedral format. Purple, red and green spheres show K, Tc, and X atoms, respectively.

Table 1 The calculated lattice constant ($a_0$ (Å)), bulk modulus ($B_0$ (GPa)), formation energy and Curie temperature $T_c$ (K) for DPs $K_2TcX_6$ (X = Cl, Br)

| Parameters | $K_2TcCl_6$ | $K_2TcBr_6$ |
|---|---|---|
| $a_0$ | 9.84 | 10.46 |
| Exp. work | 9.83[a] | |
| $B_0$ | 43.68 | 35.04 |
| $\Delta H_f$ | −1.43 | −1.28 |
| $T_c$ | 545 | 505 |

[a] Ref. 46.

compound. On the other hand, it is also evident from Table 1 that the larger electronegativity value of Cl causes it to have large value of formation energy compared to $K_2TcBr_6$. As the increasing values of $a_0$ reduces the density of the structures, the bulk modulus ($B_0$), quite contrary to $a_0$, starts decreasing from Cl to Br.

### 3.2 Curie temperature and structural stability

The graphs of the volume and augmented energy in anti-ferromagnetic (AFM) and in ferromagnetic (FM) states have been plotted in Fig. 2a–c. The estimation and comparison of the energies affirmed in Rydberg for AFM and FM states was done from the bottom. For FM, the highest omission of energy was observed as compared with AFM states. Thus, more suitability in the FM state is believed for the $K_2TcX_6$ (X = Cl, Br).

Further, formation energy helped illustrating the thermodynamic behavior while employing a reasonable chemical relation:[50]

$$\Delta H_f = E_{total}(K_aTc_bX_c) - aE_K - bE_{Tc} - cE_X \quad (1)$$

where $E_K$, $E_{Tc}$, $E_X$, are the energies of K, Tc, X atoms and $E_{total}(K_aTc_bX_c)$ are the energies of $K_2TcX_6$ (X = Cl, Br). The major contribution of atoms towards the computation remained from the *a*-Rb, *b*-Tc, and *n*-X. In FM state, the obtained values of $\Delta H_f$ for $K_2TcCl_6$ and $K_2TcBr_6$ are listed in Table 1. The energy exhausted is symbolized by the negative sign during the compound formation ensuring the thermodynamic stability of the observed compounds. Further, Br based DPs discharge less energy than that of the Cl based DP. After evaluating thermodynamic stability, it is very important to observe low Curie temperature ($T_c$) of the compounds. In this regard, Heisenberg model through the equation $T_c = 2\Delta E/3xK_B$, was brought into use where $K_B$ represents the Boltzmann constant, $x$ symbolizes the percentage of Tc and $\Delta E = E_{AFM} - E_{FM}$ shows the lowest amount of energy in the compounds. The noted values of $T_c$ for

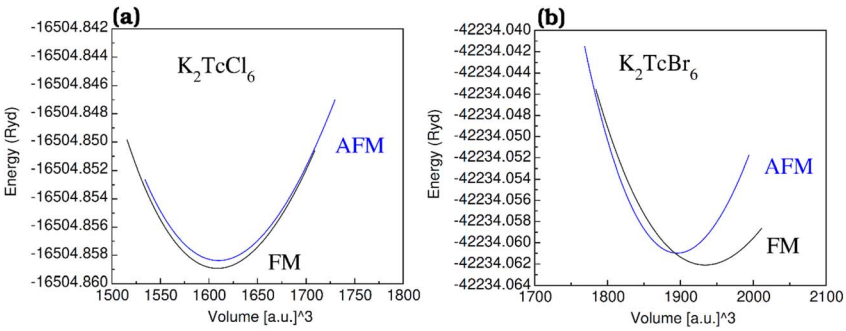


Fig. 2 The energy (in term of Ryd) *vs.* volume (in term of [a.u]$^3$) plots of double perovskites (a) $K_2TcCl_6$ and (b) $K_2TcBr_6$ in ferromagnetic (FM) and anti-ferromagnetic (AFM) phases.

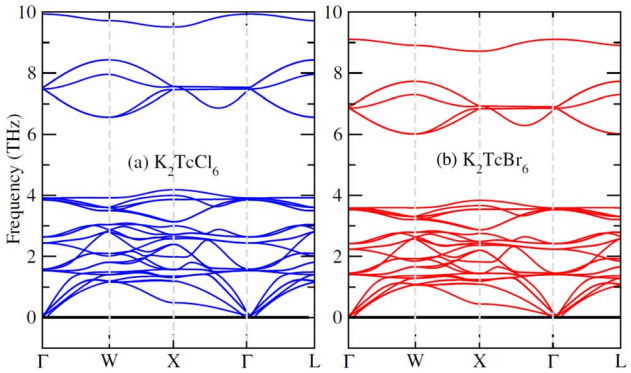


Fig. 3 Calculated phonon band structures for DPs (a) $K_2TcCl_6$ and (b) $K_2TcBr_6$.

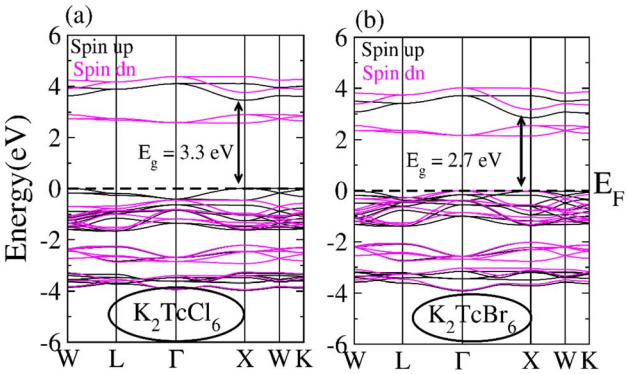


Fig. 4 Band structures calculated for (a) $K_2TcCl_6$ and (b) $K_2TcBr_6$ for spin up (black line) and spin down (pink line) using mBJ potential.

$K_2TcCl_6$ and $K_2TcBr_6$ are 545 K and 505 K. These values confirm the higher-temperature ferromagnetism for the observed compounds. The Curie temperature of $Cs_2Re(Cl/Br)_6$ and $Sr_2$-$Cr(Re/Os)O_6$ are mentioned as 635/725 K in ref. 34. We conducted calculations on phonon band structure and thermal stability for both DPs $Cs_2TcCl_6$ and $Cs_2TcBr_6$ to assess their stability. The phonon band structures for both compounds are computed and illustrated in Fig. 3a and b. The supercell approach, implemented in the PHONOPY package,[51] was utilized for these analyses. Analyzing the phonon dispersion provides insights into the phonon spectrum's band gaps. Imaginary modes in the phonon spectra signify structural dynamical instability. If the frequencies gained from the phonon spectra are imaginary, the perovskite structure is deemed unstable. In a structurally stable crystal, the absence of imaginary phonon frequencies and continuous phonon dispersion curves without gaps between optical phonon branches are expected. Gaps in these curves suggest an unstable crystal structure, indicating the existence of unrealizable vibrational modes. Such gaps often occur near the zone boundaries in the Brillouin zone and are associated with soft modes, indicating structural instabilities that can lead to phase transitions. The phonon frequencies are significantly influenced by the mass difference between atoms in a crystal lattice, as well as the force constants between the lattice structure and atoms.

### 3.3 Spin polarized electronic properties and magnetic behavior

The band structure (BS) for spin-down (↓) as well as spin-up (↑) orientations were computed using TB-mBJ potential for illustrating the ferromagnetism and spin polarization for DPs $K_2TcCl_6$ and $K_2TcBr_6$ (see Fig. 4a and b). Fermi-level ($E_F$) remains within the insulating region between conduction band (CB) and valence band (VB) of for spin-down (↓) for both DPs. On the other hands, the states stay at $E_F$ for $K_2TcCl/Br_6$ in spin-up (↑). Resultantly, our compounds exhibited semiconducting ferromagnetic DPs that is assumed a necessary factor in spintronics. Spin-up (↑) channel indicate direct bandgap nature having bandgap values are 3.3 eV and 2.7 eV for $K_2TcCl_6$ and $K_2TcBr_6$ respectively. Both double perovskites studied in this work have earlier been studied with theoretical calculations and have been shown to have band gaps above 1 eV. However, accurate determination of band gap with TB-mBJ functional has not been reported which we have done for the first time. Although no experimental data is available for comparison, our calculated values of band gaps for the two systems are better than those reported by Berri *et al.*,[52] and materials project database.[53] The larger exchange interaction value causes the larger semiconducting gap that ensures the larger ferromagnetism.

Total density of states (TDOS) along with partial density of states of Tc, K and Cl/Br atoms are calculated and represented in Fig. 5 and 6. TDOS also represent the semiconducting ferromagnetic behavior according to spin down (↓) and spin up (↑) calculated DOS. From PDOS, we see a major role of the burly hybridization of 3p/4p-Cl/Br electrons with 4-d states electrons of Tc in justifying the ferromagnetic interface [see Fig. 5 and 6].

The 4d states of Tc are sum of 4d-$t_{2g}$ and 4d-$e_g$ states. The black color from 4d states overlapped by the red and blue color in the plot of the 4d-$t_{2g}$ and 4d-$e_g$ states from which it is confirmed the complete division of the 4d states into degenerated states. The 4d-Tc states are separated in five degenerated states. Three states ($d_{zx}$, $d_{yz}$ and $d_{xy}$) out of five degenerate states recombined to triplet-$t_{2g}$-states. On the other hand, the rest of the two states ($d_{z^2}$ and $d_{x^2-y^2}$) recombined to doublet-$e_g$-states and lie at the highest energy-states. The hybridization of $t_{2g}$ states with 3p/4p-Cl/Br is found to observe at $E_F$ level in spin-up (↑). While at −3.2 eV, the hybridization of $t_{2g}$ and $e_g$ states was noted with p states of Cl/Br atom both (↓) and (↑) channels. However, the $t_{2g}$ significantly contribute to hybridization with p from −0.4 eV at $E_F$. Further, there was interaction between $t_{2g}$ states and p states of Cl/Br in (↓), which generated exchange energies ($\Delta$(d), $\Delta$(pd)) and crystal field energy ($\Delta_{CF}$). The limitations of the studied compounds for ferromagnetism are also known through these energies. The calculation of the $\Delta_{CF}$ was performed of the energy differences among degenerated states of Tc by the equation; $\Delta_{CF} = t_{2g} - e_g$. Nevertheless, $\Delta$(d) was estimated from differences of 4d states of (↓) and (↑) for Tc. The same ($\Delta$(d)) also ensured the existence of ferromagnetism. $\Delta$(d)

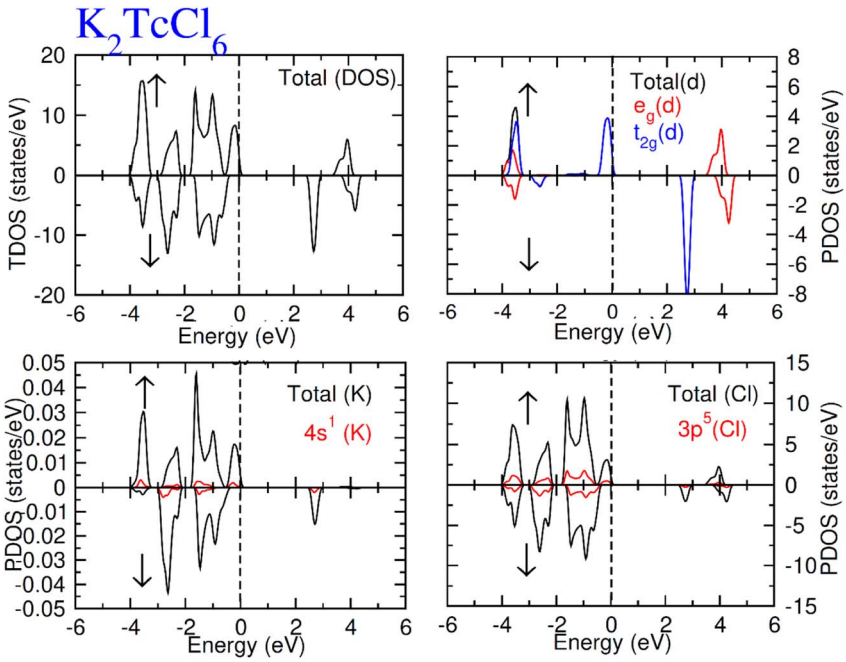


Fig. 5 Total DOS and partial DOS for DP $K_2TcCl_6$ with K, Tc and Cl atoms in spin up (↑) and spin down (↓).

holding larger value than that of $\Delta_{CF}$ (see Table 2) confirms the ferromagnetism in the compounds in hand. The stable ferromagnetism is vilified by the negative value of $\Delta$(pd), due to lower energy operating through energy forbidden region in (↓).[54]

The major contribution of the partial sub states 3p/4p of Cl/Br, 4d of Tc, and 4s of K is confirmed by the electronic arrangements of Br [Ar] $4s^2 3d^{10} 4p^5$, Cl [Ne] $3s^2 3p^5$, Tc [Kr] $4d^5 5s^2$, and K [Ar] $4s^1$. The band edge splitting at CB and VB caused by the mentioned partially filled states are represented as exchange constants ($N_o\beta$ and $N_o\alpha$). The p–d interactions are attributed to $N_o\beta$ whereas s–d states interactions are related to $N_o\alpha$ by the relation as under:

$$N_o\alpha = \frac{\Delta E_C}{x\langle S\rangle} \quad (2)$$

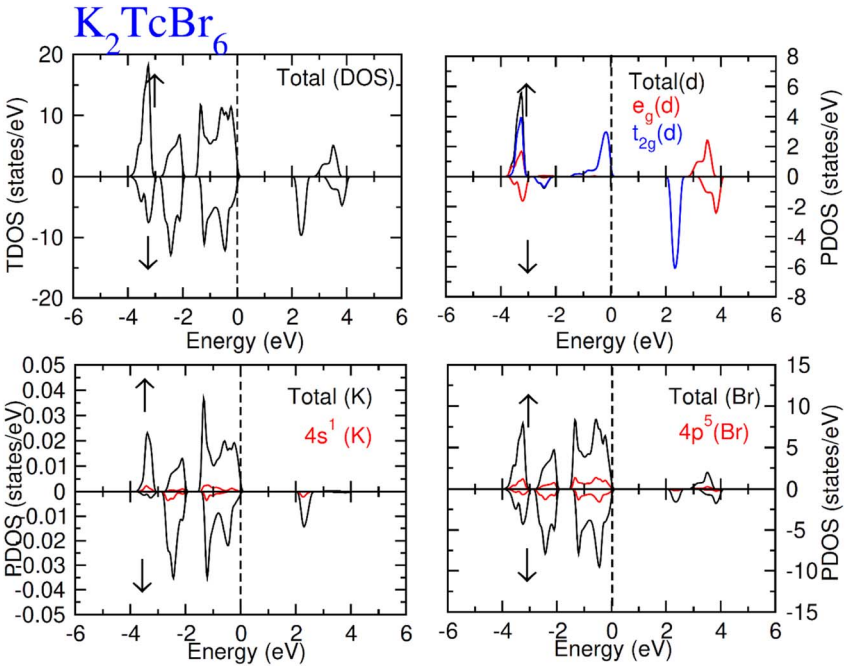


Fig. 6 Total DOS and partial DOS for DP $K_2TcBr_6$ with K, Tc and Br atoms in spin up (↑) and spin down (↓).

Table 2 Computed crystal field energy, exchange splitting $\Delta_x$(d), p–d exchange constant ($N_o\beta$) and s–d exchange-constant ($N_o\alpha$) for DPs $K_2TcX_6$ (X = Cl, Br)

| Parameters | $K_2TcCl_6$ | $K_2TcBr_6$ |
|---|---|---|
| $\Delta E_{cry}$ | 3.2 | 2.9 |
| $\Delta_x$(d) | 5.4 | 5.0 |
| $\Delta_x$(pd) | −0.6 | −0.4 |
| $N_o\alpha$ | −0.39 | −0.33 |
| $N_o\beta$ | −0.53 | −0.38 |

$$N_o\beta = \frac{\Delta E_V}{x\langle S\rangle} \quad (3)$$

The $\Delta E_V$ is the valence band edge (VBE) difference whereas $\Delta E_C$ is the conduction band edge (CBE) difference for (↓) and (↑) channels. $x$ represents the concentration of Tc and $\langle S\rangle$ is symbolized for the value of magnetic moment.[55,56] $N_o\beta$ remains negative whereas $N_o\alpha$ stays positive for normal wave functions that become just like stationary waves afterwards, which reverts the sign of $N_o\alpha$, by being trapped into deep potential through quantum confinement effect, (see Table 2). The exchange mechanism helps lowering the energy of the compounds while stabilizing the ferromagnetism; hence, the $N_o\beta$ becomes more outstanding for ferromagnetism. Our results show that exchange mechanism is responsible for ferromagnetic interaction for the two double perovskites. This is based on the computed s–d exchange-constant ($N_o\alpha$), p–d exchange constant ($N_o\beta$), exchange splitting $\Delta_x$(d) and crystal field energy for DPs $K_2TcX_6$ (X = Cl, Br) reported in Table 2.

The role electronic spins in magnetic moment (MM) along FM for $K_2TcCl_6$ and $K_2TcBr_6$ is explained in Table 3. The absolute polarization is shown by the integer values of MM. Further, the exchange of electrons spin is confirmed by the electronic shift from Tc to K, Cl/Br. In addition, Tc and MM is increased by the empty places at Tc, which becomes their outstanding properties for spintronics. The solitude electrons configuration along with MM connects neighboring polarized atoms, increasing broad-range FM through RKKY exchange model.[57] The shift of MM towards nonmagnetic sites (Rb, Cl/Br) from magnetic elements (Tc) is generated by the hybridization between 3p/4p-Cl/Br and 4d-Tc. The ferromagnetism is shown for $Cs_2MoCl_6$ along with node ring electrons in BS.[58] The potency of spin–orbit coupling of $A_2TaCl_6$ because of octahedral of halogen ions and substantial ionicity, $J_{eff} = 3/2$ of 5d was studied by Ishikawa *et al.*[59] Consequently, 100% spin polarization is exhibited by the integer values of MM, which is the major contribution of Tc (see Table 3).

Table 3 The calculated values of magnetic moments, $M$ for DPs $K_2TcX_6$ (X = Cl, Br)

| Parameters | $K_2TcCl_6$ | $K_2TcBr_6$ |
|---|---|---|
| $M_{tot}$ ($\mu_B$) | 2.999 | 2.999 |
| $M_K$ ($\mu_B$) | 0.006 | 0.008 |
| $M_{Tc}$ ($\mu_B$) | 2.259 | 2.215 |
| $M_{Cl/Br}$ ($\mu_B$) | 0.061 | 0.056 |
| $M_{Int}$ ($\mu_B$) | 0.373 | 0.442 |

### 3.4 Optical properties

Fig. 7a–f show the elaboration of the optical parameters, which depend on bandgap (BG). These compounds become very imperative for being utilized in optoelectronics just because of having direct BG of ferromagnetic DPs $K_2TcX_6$ as it limits the de-excitation along with direct electronic transition to CB from VB. In addition, changeability in band gap further formulates them for being employed in a range of other device applications. $K_2TcBr_6$ and $K_2TcCl_6$ possessing the values of absorption of light energy 2.7 eV and 3.3 eV for BGs goes down in UV and visible spectrum.[60,61] The optical parameters have been analyzed in the form of real as well as imaginary parts of dielectric constants $\varepsilon_1(\omega)$ and $\varepsilon_2(\omega)$. The polarization and dispersion of light is symbolically and quantitatively measured by $\varepsilon_1(\omega)$. Fig. 7a clearly displays its observed value $\varepsilon_1(\omega)$ at $\omega = 0$, reaching at 3.9 after increasing from 3.2 when Cl was changed to Br. The increasing value of $\varepsilon_1(0)$ due to changing the halide ions causes the reduction in BG from 3.3 to 2.7 exactly satisfying the Penn's model $\varepsilon_1(0) \approx 1 + (\hbar\omega_p/E_g)^2$.[62] The polarization and dispersion of light energy becomes comparatively high due to resonance peaks of the $\varepsilon_1(\omega)$ that have different peak sets, as at 4.3/3.0 eV and at 2.5/1.0 eV. The variation in refractive index $n(\omega)$ also changes the speed decay of light while passing through compounds. The behavior of $\varepsilon_1(\omega)$ and $n(\omega)$ has also been proven to be alike (see Fig. 7b). The $n(0)$ has been observed through the equation $n(0) = (\varepsilon_1(0))^{1/2}$, (see Table 1). The change of anions enhances the values of $n(0)$, however, largely the relation with $\varepsilon_1(0)$ remains secured. Further, Krammer–Kronge formulism was used to determine $\varepsilon_2(\omega)$ from $\varepsilon_1(\omega)$.[63] The absorbed light energy in a compound is symbolized by $\varepsilon_2(\omega)$. Therefore, its higher value due to huge absorption is believed to be incredible for optoelectronic applications. It obtained value has been displayed in Fig. 7c. Its critical values were recorded as 2.2 eV and 3.2 eV showing the band gap of $K_2TcBr_6$ and $K_2TcCl_6$ correspondingly. Similarly, the absorption bands observed for $K_2TcBr_6$ and $K_2TcCl_6$ are 2.5 to 3.5 eV and 4.0 to 4.5 eV accordingly. $K_2TcBr_6$ is certified by the recorded bands for visible regions and $K_2TcCl_6$ for UV as well. The absorption bands were also formed by the electronic transitions at 3.8 eV onwards, 3.0 to 4.0 eV and 4.2 to 4.8 eV. However, generally the first absorption bands are strongly preferred for optoelectronics.

Fig. 7d shows the recorded values of absorption coefficient $\alpha(\omega)$. A similar trend of $\alpha(\omega)$ as that of $\varepsilon_2(\omega)$ was found to observe. It was so because the both ($\alpha(\omega)$ and $\varepsilon_2(\omega)$) have representation of absorption of light. There is also a bit overestimation in the obtained values of absorptions and optical bands gap due to DFT. When Cl is replaced by Br, the absorption bands move towards lower energy. The modeling of band gap causes this shift towards lower values. The $k(\omega)$ represents to be the fictional of refraction as $\varepsilon_2(\omega)$. It represents the decayed part of light energy (see Fig. 7d). In addition, it has two

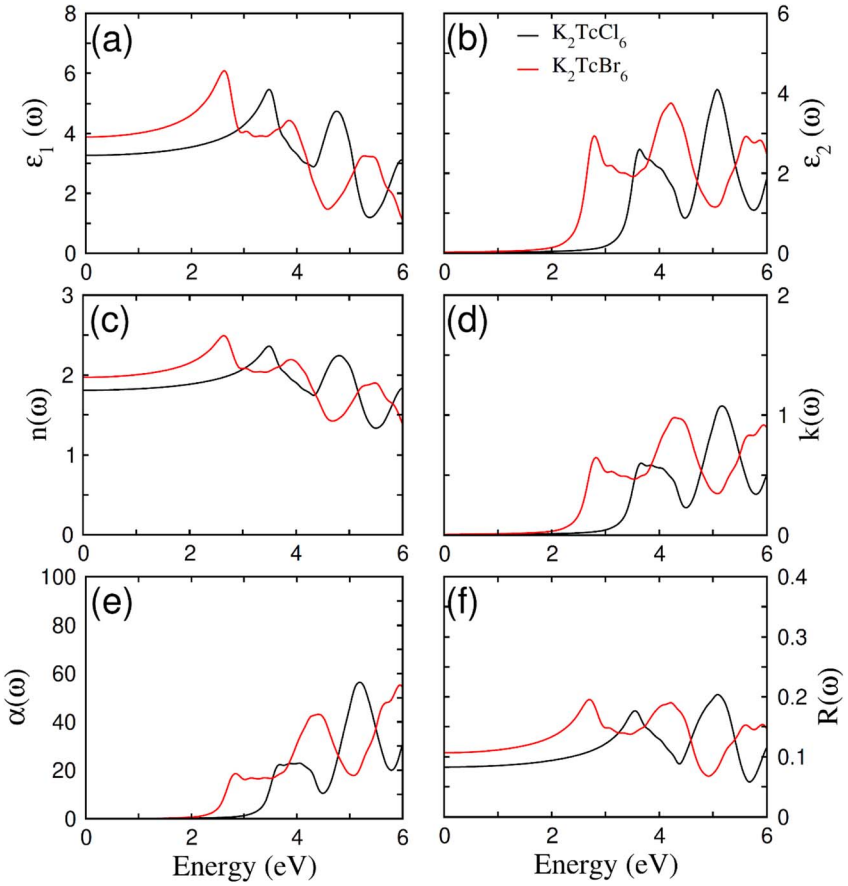


Fig. 7 The calculated (a) real part $\varepsilon_1(\omega)$, (b) imaginary part $\varepsilon_2(\omega)$, (c) refraction $n(\omega)$, (d) extinction co-efficient $k(\omega)$, (e) absorption $\alpha(\omega)$, (f) reflectivity $R(\omega)$ of DPs $K_2TcCl_6$ and $K_2TcBr_6$.

consecutive sets of peaks; the first one at 2.8/4.4 and the second one at 3.6/5.2 for Br/Cl correspondingly. The obtained values proved to be in accordance with $\varepsilon_2(\omega)$ and $\alpha(\omega)$.[64] The reflected part of energy from the surface of the compound is known as reflectivity $R(\omega)$. Its frequency dependent value and static value $R(0)$ have been expressed in Fig. 7f. Its static value $R(0)$ started increasing by replacing the Cl with Br. The uppermost peak value of $R(\omega)$ remained below 0.21 that was much smaller as compared with the absorption of light energy in the compounds.

### 3.5 Thermoelectric properties

Thermoelectric features are generally investigated for the better understanding of their effects on thermoelectric performance and electronic spin in specific compounds. Any thermoelectric compound is believed to possess heavier elements to restrain the phonons transport.[65,66] The ideal thermoelectric compounds also possess ultralow thermal conductivity ($\kappa_e$), electric conductivity ($\sigma$), and extensive Seebeck coefficient ($S$). The temperature limit for the computed parameters is from 200 K to 800 K. In this regard, power factor ($\sigma S^2$) was computed to assay the performance of DPs $K_2TcCl_6$ and $K_2TcBr_6$. In accordance with the classical Boltzmann theory, the collision rate of time for electronic gas was set as $10^{-14}$ s. Thus, the division of the $\kappa_e$ and the $\sigma$ was taken in terms of $10^{-14}$ s [see Fig. 8a–f]. The combination of all three parameters ($\kappa_e$, $\sigma$, $S$) for ($\downarrow$) and ($\uparrow$) is taken by the following equation:[47]

$$\kappa = \kappa(\uparrow) + \kappa(\downarrow)/2 \quad (4)$$

$$S = S(\uparrow)\sigma(\uparrow) + S(\downarrow)\sigma(\downarrow)/\sigma(\uparrow) + \sigma(\downarrow) \quad (5)$$

The above written relation shows the means of the both spin formations. Fig. 8a shows the computed values of $\sigma$. There is a difference between the thermoelectric factors of Tc based double perovskites as Tc possesses the electrons in odd numbers (5) in 4d orbitals. Its values increases at 200 K and 800 K from $0.6/0.3 \times 10^{19}$ ($\Omega^{-1}$ m$^{-1}$ s$^{-1}$) to $0.9/1.6 \times 10^{19}$ ($\Omega^{-1}$ m$^{-1}$ s$^{-1}$) respectively. The values of $\sigma$ are more for Br based DPs than that of Cl based DPs at 400–800 K. It is so because the free carriers are increased in numbers by increasing the size of ions. Quite contrary to the values of $\sigma$, the $\kappa_e$ starts increasing at 200 K to 800 K from $0.4/0.5 \times 10^{14}$ W m$^{-1}$ K$^{-1}$ s$^{-1}$ to $1.9/5.5 \times 10^{14}$ W m$^{-1}$ K$^{-1}$ s$^{-1}$ for $K_2Tc(Cl/Br)_6$. It is so because the lattice disturbance and the flow of carriers is increased by thermal effect (see Fig. 8c). Here, due to the restrictions of classical theory of Boltzmann, the merely electronic contribution to thermal conductivity was investigated whereas we could not

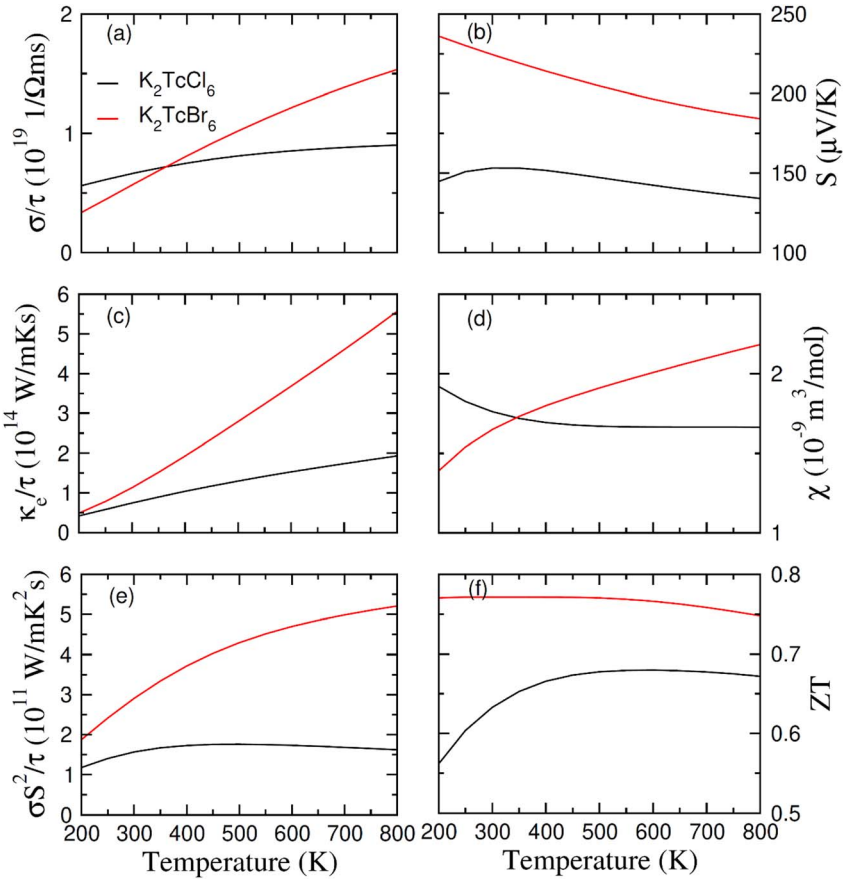


Fig. 8 The computed (a) electrical conductivity ($\sigma/\tau$), (b) thermal conductivity ($k_e/\tau$), (c) Seebeck coefficients ($S$), (d) specific heat capacity ($C_v$), (e) power factor and (f) figure of merit against temperature for DPs $K_2TcCl_6$ and $K_2TcBr_6$.

touch the lattice disturbance. The comparison of $\sigma$ and $\kappa_e$ was performed through the $\kappa/\sigma$ that is set as $10^{-6}$ in order to evaluate the relative effect.[67] The ultralow values of $\kappa_e$ provide the room for the compounds to be the best for spintronic and thermoelectric projects.

The potential gradient for thermoelectric measured through $S$ is presented in Fig. 8b. The value of $S$ became positive for $K_2Tc(Cl/Br)_6$ at 200–800 K, showing the p-type character. With increasing temperature from 200 K to 800 K, the values of $S$ reduced from 148/230 mV $K^{-1}$ to 130/180 mV $K^{-1}$ for $K_2Tc(Cl/Br)_6$. The variation of the susceptibility of $K_2Tc(Cl/Br)_6$ as depicted in Fig. 8d, manifest an opposite trend. For $K_2TcCl_6$, the value of $\chi$ decreases up to 400 K then becomes constant to reach approximately value of $1.6 \times 10^{-9}$ $m^3$ $mol^{-1}$ at 800 K. For $K_2TcCl_6$, the value of $\chi$ increases steadily up to 800 K then attains almost a steady approximately value of $2.3 \times 10^{-9}$ $m^3$ $mol^{-1}$.

From the analysis of the computed values of power factor (PF) (see Fig. 8e), it is clear that its values are lowest for $K_2TcCl_6$ and highest for $K_2TcBr_6$. Therefore, Br based DP is believed to be more suitable for being used in thermoelectric device applications as compared with the Cl based DP. Additionally, the PF, mathematically equivalent to $\sigma S^2$, is calculated consequently, by utilizing these Seebeck coefficients in conjunction with the structural factor, one can determine the figure of merit, which fundamentally characterizes the efficacy of any thermoelectric material. When calculating the thermal efficiency ($ZT$) (see Fig. 8f), it exhibited a pattern similar to that of PF, for both studied DPs. This underscores the potential of both DPs as promising thermoelectric materials for a wide array of thermoelectric purposes.

## 4. Conclusion

To sum up, we have conducted a systematic evaluation of ferromagnetism and its impact on the functionality of electrons in the double perovskites (DPs) $K_2TcY_6$ (Y = Cl, Br) with the aim of exploring their potential applications in energy harvesting and spintronic devices. Primarily, our examination of cubic spinel structures of the investigated double perovskites in both ferromagnetic (FM) and antiferromagnetic (AFM) states has affirmed that with higher energy release the FM states are more energetically stable. Their structural and thermodynamic stability in FM states has also been corroborated by the tolerance factor and formation energy assessment. Moreover, the Heisenberg model corroborates that Tc remains above room temperature, while the larger exchange-energies in comparison to crystal field energy, coupled with the double exchange model,

point towards the presence of ferromagnetism resulting from spin functionality and hybridization, as opposed to clustering. The prevailing negative exchange-constants exert a significant influence through the quantum confinement effect, effectively confining the electron wavefunction within a deep potential well. This negative pd exchange-interaction, coupled with the shift of magnetic moments from Tc to the K and Cl/Br sites, is a result of exchange mechanism that reduces the system's energy and bolsters the stability of ferromagnetism. From our results it can be seen that the band gaps of $K_2TcBr_6$ and $K_2TcCl_6$ are 2.2 eV and 3.2 eV, respectively. Since these values are in the UV region, one can expect these materials to be suitable for optical devices operating in UV region of electromagnetic spectrum. Absorption spectra have been observed in both the UV and visible regions for double perovskites containing Cl and Br anions. Furthermore, the presence of unpaired electrons in Tc enhances electrical conductivity and the performance of $K_2TcBr_6$-based double perovskites surpasses that of $K_2TcCl_6$-based DP. Moreover, our computed properties exhibit semiconducting ferromagnetic DPs that is assumed a necessary factor in spintronics devices.

## Conflicts of interest

There are no conflicts to declare.

## Acknowledgements

The authors express their gratitude to Princess Nourah Bint Abdulrahman University Researchers Supporting Project (Grant No. PNURSP2024R70), Princess Nourah Bint Abdulrahman University, Riyadh, Saudi Arabia.

## References

1 T. Dietl, A ten-year perspective on dilute magnetic semiconductors and oxides, *Nat. Mater.*, 2010, **9**, 965.
2 S. Bhatti, R. Sbiaa, A. Hirohata, H. Ohno, S. Fukami and S. N. Piramanayagam, Spintronics based random access memory: a review, *Mater. Today*, 2017, **20**(9), 530–548.
3 I. Žutić, J. Fabian and S. Das Sarma, Spintronics: Fundamentals and applications, *Rev. Mod. Phys.*, 2004, **76**(2), 323–410.
4 G. A. Medvedkin, T. Ishibashi, T. Nishi and K. Hayata, Room temperature ferromagnetism in novel diluted magnetic semiconductor Cd1-xMnxGeP2, *Jpn. J. Appl. Phys.*, 2000, **39**, L949.
5 S. D. Sarma, Spintronics: A new class of device based on electron spin, rather thanon charge, may yield the next generation of microelectronics, *Am. Sci.*, 2001, **89**, 516.
6 K. Ando, Seeking room-temperature ferromagnetic semiconductors, *Science*, 2006, **312**, 1883–1885.
7 T. Dietl, H. Ohno, F. Matsukura, J. Cibert and D. Ferrand, Zener model description of ferromagnetism in zinc-blende magnetic semiconductors, *Science*, 2000, **287**, 1019–1022.
8 P. Sharma, A. Gupta, K. V. Rao, F. J. Owens, R. Sharma, R. Ahuja, J. M. O. Guillen, B. Johansson and G. A. Gehring, Ferromagnetism above room temperature in bulk andtransparent thin films of Mn-doped ZnO, *Nat. Mater.*, 2003, **2**(10), 673–677.
9 R. K. Kittilstved, N. S. Norberg and D. R. Gamelin, Chemical manipulation of high-Tcferromagnetism in ZnO diluited magnetic semiconductor, *Phys. Rev. Lett.*, 2005, **94**, 147209.
10 A. Sundaresan, R. Bhargavi, N. Rangarajan, U. Siddesh and C. N. R. Rao, Ferromagnetism as a universal feature of nanoparticles of the otherwisenonmagnetic oxides, *Phys. Rev. B: Condens. Matter Mater. Phys.*, 2006, **74**, 161306(R).
11 D. Sanyal, M. Chakrabarti, T. K. Roy and A. Chakrabarti, The origin of ferromagnetismand defect-magnetization correlation in nanocrystalline ZnO, *Phys. Lett. A*, 2007, **371**(5–6), 482–485.
12 H. Pan, J. B. Yi, L. Shen, R. Q. Wu, J. H. Yang, J. P. Feng, J. Ding, L. H. Van and J. H. Yin, Room-temperature ferromagnetism in carbon-doped ZnO, *Phys. Rev. Lett.*, 2007, **99**, 127201.
13 H. Luitel, P. Chettri, A. Tiwari and D. Sanyal, Experimental and first principle study of room temperature ferromagnetism in carbon-doped rutile TiO2, *Mater. Res. Bull.*, 2019, **110**, 13–17.
14 H. Luitel, M. Chakrabarti, A. Sarkar, S. Dechoudhury, D. Bhowmick, V. Naik and D. Sanyal, Ab-initio calculation and experimental observation of room temperatureferromagnetism in 50 keV nitrogen implanted rutile TiO2, *Mater. Res. Express*, 2018, **5**, 026104.
15 H. Luitel and D. Sanyal, Ab initio calculation of magnetic properties in B, Al, C, Si, N, Pand As-doped rutile TiO2, *Int. J. Mod. Phys. B*, 2017, **31**, 1750227.
16 H. Luitel, S. Roy and D. Sanyal, Ab-initio calculation of magnetic properties of P and Asdoped SnO2, *Computational Condensed Matter*, 2018, **14**, 36–39.
17 H. Luitel and D. Sanyal, Ferromagnetism in p-block elements doped ZnO: An ab-initio approach, *Computational Condensed Matter*, 2019, **19**, 00376.
18 H. Luitel, S. Roy, M. Chakrabarti, P. Chettri, A. Tiwari, V. Naik and D. Sanyal, Room temperature ferromagnetism in boron-doped oxides: a combined first-principle and experimental study, *Philos. Mag. Lett.*, 2020, **100**(4), 141–153.
19 S. Wang, L. Pan, J.-J. Song, W. Mi, J.-J. Zou, L. i. Wang and X. Zhang, Titanium defected undoped anatase tio 2 with p-type conductivity, room-temperature ferromagnetism, and remarkable photocatalytic performance, *J. Am. Chem. Soc.*, 2015, **137**(8), 2975–2983.
20 D. Sanyal, M. Chakrabarti, P. Nath, A. Sarkar, D. Bhowmick and A. Chakrabarti, Room temperature ferromagnetic ordering in 4 MeV Ar5+ irradiated TiO2, *J. Phys. D: Appl. Phys.*, 2013, **47**, 025001.
21 H. Luitel, A. Sarkar, M. Chakrabarti, S. Chattopadhyay, K. Asokan and D. Sanyal, Positron annihilation lifetime characterization of oxygen ion irradiated rutile TiO2, *Nucl. Instrum. Methods Phys. Res., Sect. B*, 2016, **379**, 215–218.
22 M. Venkatesan, C. B. Fitzgerald and J. M. D. Coey, Unexpected magnetism in a dielectric oxide, *Nat. Commun.*, 2004, **430**, 630.

23 J. M. D. Coey, ferromagnetism, *Solid State Sci.*, 2005, **7**(6), 660–667; R. Masrour, E. K. Hlil, M. Hamedoun and A. Benyoussef, Electronic and magnetic properties of MnAu nanoparticles, *J. Magn. Magn. Mater.*, 2014, **354**, 159–162.

24 H. H. Fang, R. Raissa, M. Abdu-Aguye, S. Adjokatse, G. R. Blake, J. Even and M. A. Loi, Photophysics of organic-inorganic hybrid Lead iodide perovskite single crystals, *Adv. Funct. Mater.*, 2015, **25**, 2346–2347.

25 H. Z. Lin, C. Y. Hu, P. H. Lee, A. Z. Z. Yan, *et al.*, Half-metallic property induced by double exchange interaction in the double perovskite Bi2BB′O6 (B, $B'$ = 3d transitional metal) via first-principles calculations, *Materials*, 2019, **12**, 1844.

26 H. E. M. Musa Saad and S. S. Althoyai, Half-metallic and insulating natures in Ru-based ordered double perovskite oxides Ba2XIIIRuVO6 (X = V, Cr) induced by 3d-t2gn orbital filling, *Mater. Chem. Phys.*, 2017, **190**, 230–240.

27 A. Hossain, P. Bandyopadhyay and S. Roy, An overview of double perovskites A2B′ B″ O6 with small ions at A site: synthesis, structure and magnetic properties, *J. Alloys Compd.*, 2018, **740**, 414–427.

28 K. I. Kobayashi, T. Kimura, H. Sawada, K. Terakura and Y. Tokura, Room-temperature magnetoresistance in an oxide material with an ordered double-perovskite structure, *Nature*, 1998, **395**, 677.

29 Y. Krockenberger, K. Mogare, M. Reehuis, M. Tovar, M. Jansen and G. Vaitheeswaran, Sr2CrOsO6: end of a spin-polarized metal-insulator transition by 5d band filling, *Phys. Rev. B: Condens. Matter Mater. Phys.*, 2007, **75**, 020404.

30 S. Ravi, High Curie temperature and room temperature magnetoresistance in Pr2FeCrO6 material for spintronics applications, *Mater. Lett.*, 2020, **278**, 128448.

31 O. Ramdane, M. Labidi, R. Masrour, S. Labidi, M. Ellouze and R. Rehamnia, Study of structural, electronic, and magnetic properties of cubic and tetragonal Ba2FeMoO6, *J. Supercond. Novel Magn.*, 2023, **36**, 373–387.

32 M. Bessimou and R. Masrour, Magnetocaloric effect and magnetic properties of Dy2CoMnO6: Monte Carlo study, *Philos. Mag.*, 2023, **103**, 56–66.

33 A. E. Maughan, A. M. Ganose, D. O. Scanlon and D. O. Neilson, Perspectives and design principles of vacancy-ordered double perovskite halide semiconductors, *Chem. Mater.*, 2019, **31**, 1184–1195.

34 Q. Mahmood, G. Nazir, A. Rahim, J. Alzahrani, A. I. Aljameel, G. Murtaza, A. Aldayyat, H. Albalawi, A. Mera and B. Ul Haq, Impact of 5d electrons on half metallic ferromagnetism, and thermoelectric properties of Cs2Z(Cl/Br)6 (Z = Os, Ir) for spintronic applications, *Mater. Chem. Phys.*, 2022, **288**, 126414.

35 M. B. Gray, J. D. Majher, N. P. Holzapfel and P. M. Woodward, Exploring the stability of mixed-halide vacancy-ordered quadruple perovskites, *Chem. Mater.*, 2021, **33**, 2165–2172.

36 M. M. S. Karim, A. M. Ganose, L. Pieters, W. W. W. Leung, J. ade, L. Zhang, D. O. Scanlon and R. G. Palgrave, Anion distribution, structural distortion, and symmetry-driven optical band gap bowing in mixed halide Cs2SnX6 vacancy ordered double perovskites, *Chem. Mater.*, 2019, **31**, 9430–9444.

37 B. Lee, A. Krenselewski, S. I. Baik, D. N. Seidman and R. P. H. Chang, Solution processing of air-stable molecular semiconducting iodosalts, Cs2SnI6−xBrx, for potential solar cell applications, *Sustainable Energy Fuels*, 2017, **1**(4), 710–724.

38 A. E. Maughan, A. M. Ganose, M. M. Bordelon, E. M. Miller, D. O. Scanlon and J. R. Neilson, Air-stable molecular semiconducting iodosalts for solar cell applications: Cs2SnI6 as a hole conductor, *J. Am. Chem. Soc.*, 2016, **138**, 8453–8464.

39 M. Faizan, S. H. Khan, G. Murtaza, A. Khan and A. Laref, Electronic and magnetic properties of alkali metal chlorides A2MCl6 (A = K, Rb, Cs; M = Mn, Mo): a density functional theory study, *Int. J. Mod. Phys. B*, 2019, **33**, 1950072.

40 Q. Mahmood, First-principles calculations to investigate role of 4d electrons spin (Mo/Tc) in half metallic ferromagnetism, and thermoelectric characteristics of $Rb_2$(Tc, Mo)$X_6$ (X =Cl, Br), *Ceram. Interfaces*, 2023, **49**, 25121–25129.

41 G. M. Mustafa, M. Hassan, N. M. Aloufi, S. Saba, S. Al-Qaisi, Q. Mahmood, H. Albalawi, S. Bouzgarrou, H. H. Somaily and A. Mera, Half metallic ferroamgnetism, and transport properties of vacancy ordered double perovskites $Rb_2$(Os/Ir)$X_6$ (X= Cl, Br) for spintronic application, *Ceram. Interfaces*, 2022, **48**, 23460–23467.

42 R. Ullah, M. A. Ali, G. Murtaza, A. Khan and A. Mahmood, Ab initio study for the structural, electronic, magnetic, optical, and thermoelectric properties of K2OsX6 (X = Cl, Br) compounds, *Int. J. Energy Res.*, 2020, **44**, 9035–9049.

43 M. A. Ali, G. Murtaza and A. Laref, Exploring the ferromagnetic half metallic nature of Cs2NpBr6 via spin polarized density functional theory, *Chin. J. Phys.*, 2020, **29**, 066102.

44 K. Radja, B. L. Farah, A. Ibrahim, D. Lamia, I. Fatima, *et al.*, Investigation of structural, magneto-electronic, elastic, mechanical and thermoelectric properties of novel lead-free halide double perovskite Cs2AgFeCl6: first-principles calculations, *J. Phys. Chem. Solids*, 2022, **167**, 110795–110802.

45 A. Gherriche, A. Bouhemadou, Y. Al-Douri, S. Bin-Omran, R. Khenata and M. A. Hadi, Ab initio exploration of the structural, elastic, electronic and optical properties of a new layered perovskite-type oxyfluoride: CsSrNb2O6F, *Mater. Sci. Semicond. Process.*, 2021, **131**, 105890–105900.

46 M. Elder, J. E. Fergusson, G. J. Gainsford, J. H. Hickford and B. R. Penfold, Potassium pentachlorohydroxytechnetate(iv), *J. Chem. Soc. A*, 1967, 1423–1425.

47 G. K. H. Madsen and D. J. Singh, BoltzTraP. A code for calculating band-structure dependent quantities, *Comput. Phys. Commun.*, 2006, **175**, 67–71.

48 P. Blaha, K. Schwarz, G. Madsen, D. Kvasnicka and J. Luitz, *WIEN2k, an Augmented Plane Wave Plus Local Orbitals*

*Program for Calculating Crystal Properties*, Vienna University of Technology, Austria, 2001.

49 F. Tran and P. Blaha, Accurate band gaps of semiconductors and insulators with a semilocal exchange-correlation potential, *Phys. Rev. Lett.*, 2009, **102**, 226401.

50 F. Tran Koller and P. Blaha, Merits and limits of the modified Becke-Johnson exchange potential, *Phys. Rev. B: Condens. Matter Mater. Phys.*, 2011, **83**, 195134.

51 W. Yi, G. Tang, X. Chen, B. Yang and X. Liu, qvasp: A flexible toolkit for VASP users in materials simulations, *Comput. Phys. Commun.*, 2020, **257**, 107535.

52 S. Berri and N. Bouarissa, Electronic Structure and Optical Spectra of Halide Perovskites A2BCl6 [(A= Cs; B= Se, Sn, Te, Ti, Zr) and (A= K; B= Pd, Pt, Sn)] for Photovoltaic and Optoelectronic Applications, *Phys. Status Solidi B*, 2023, 2300280.

53 A. Jain, S. P. Ong, G. Hautier, W. Chen, W. D. Richards, S. Dacek, S. Cholia, D. Gunter, D. Skinner, D. Ceder and K. A. Persson, Commentary: The Materials Project: A materials genome approach to accelerating materials innovation, *APL Mater.*, 2013, **1**, 011002.

54 C. W. Zhang and S. Yan, First-principles prediction of half-metallic ferromagnetism inCu-doped ZnS, *J. Appl. Phys.*, 2010, **107**, 043913.

55 Y. F. Li, K. C. Zhang and Y. Liu, Spin-orbital coupling, and magnetic properties of Irbaseddouble perovskites with different 5dn (n = 3, 4, 5) states, *Phys. Lett.*, 2019, **383**, 558–565.

56 Q. Mahmood, S. A. Ali, M. Hassan and A. Laref, First principles study offerromagnetism, optical and thermoelectric behaviors of AVO3 (A = Ca, Sr, Ba) perovskites, *Mater. Chem. Phys.*, 2018, **211**, 428–437.

57 L. Brey, M. J. Calderón, S. Das Sarma and F. Guinea, Mean-field theory for doubleperovskites: coupling between itinerant electron spins and localized spins, *Phys. Rev. B: Condens. Matter Mater. Phys.*, 2006, **74**, 094429.

58 T. Zhang, D. Hara and S. Murakami, Unique surface-state connection between Weyland nodal ring fermions in ferromagnetic material Cs2MoCl6, *Phys. Rev. Res.*, 2021, **3**, L042037.

59 H. Ishikawa, T. Takayama, R. K. Kremer, J. Nuss, R. Dinnebier, K. Kitagawa, K. Ishii and H. Takagi, Ordering of hidden multipoles in spin-orbit entangled 5d1 Tachlorides, *Phys. Rev. B*, 2019, **100**, 045142.

60 T. H. Flemban, V. Singaravelu, A. A. S. Devi and I. S. Roqan, Homogeneous vertical ZnOnanorod arrays with high conductivity on an in situ Gd nanolayer, *RSC Adv.*, 2015, **5**(115), 94670–94678.

61 B. Xin, N. Alaal, S. Mitra, A. Subahi, Y. Pak, D. Almalawi and N. Alwadai, Identifyingcarrier behavior in ultrathin indirect-bandgap CsPbX3 nanocrystal films for use inUV/visible-blind, *Small*, 2020, **16**(43), 2004513.

62 D. R. Penn, Wave-number-dependent dielectric function of semiconductors, *Phys. Rev.*, 1962, **128**, 2093–2097.

63 S. Al-Qaisi, R. Ahmed, B. U. Haq, D. Rai and S. Tahir, A comprehensive first-principlescomputational study on the physical properties of lutetium aluminum perovskiteLuAlO3, *Mater. Chem. Phys.*, 2020, **250**, 123148.

64 B. U. Haq, S. AlFaify, T. A. Alrebdi, R. Ahmed, S. Al-Qaisi, M. Taib, G. Naz and S. Zahra, Investigations of optoelectronic properties of novel ZnO monolayers: A firstprinciplesstudy, *Mater. Sci. Eng., B*, 2021, **265**, 115043.

65 D. Singh, M. Sajjad, J. A. Larsson and R. Ahuja, *Results Phys.*, 2020, **19**, 103584.

66 N. Tayebi, K. Bidai, M. Ameri, S. Amel, I. Ameri, Y. Al-Douri and D. Varshney, Pressureand temperature dependence of the structural, elastic, and thermodynamicproperties of potassium telluride: first-principles calculations, *Chin. J. Phys.*, 2017, **55**, 769–779.

67 B. Ul Haq, S. AlFaify, T. Alshahrani, R. Ahmed, Q. Mahmood, D. M. Hoat and S. A. Tahir, Investigations of thermoelectric properties of ZnO monolayers from thefirst-principles approach, *Phys. E*, 2021, **126**, 114444.